



INTERNATIONAL JOURNAL OF ENGINEERING SCIENCES & RESEARCH TECHNOLOGY

Synthesis and Characterization of Biomaterial Hydroxyapatite

Ramandeep Singh*, Jagteshwar Singh Sidhu

*Assistant Professor, Department of Mechanical Engineering, Chandigarh Engineering College,
Chandigarh Group of Colleges, Landran, Punjab, India

Assistant Professor, Department of Mechanical Engineering, Maharaja Agarsen University, Atal Shiksha
Kunj, Baddi, Himachal Pradesh, India

jts_sidhu@yahoo.com

Abstracts

Hydroxyapatite (HA) is successfully used as a bio implant material because it resembles the bone apatite up to a great extent and possesses good biocompatibility. In the present study, HA powder has been synthesized by sol-gel technique. The as prepared powder was sintered at two different temperatures 400°C and 750°C to increase its crystallinity. A HA-CNT composite sample was also prepared to compare the results. The final sintered powder was characterized by X-ray diffraction analysis, Scanning Electron Microscopy (SEM) to know about its phase content and morphology. Thermal Analysis (TGA-DTA) was carried out to study the stability of the powder with respect to temperature. Energy Dispersive Spectroscopy (EDS) was carried out to get the information about the elements present in the final powder and their respective weight percentage. The XRD pattern indicated the formation of Ca₅HO₁₃P₃ and Ca₂H₈O₁₁P₂ phases. The higher temperature sintering of the as prepared samples leads to the good crystallinity. On the other hand, the powder sintered at 400°C could not show any crystalline phase formation. Moreover, the addition of CNTs increased the crystallinity and crystallite size of the powder.

Keywords: CNT, EDS, Hydroxyapatite, SEM, TGA-DTA, XRD.

Introduction

Hydroxyapatite: Hydroxyapatite is the calcium phosphate complex which is the main mineral of bones. It is the crystallized form of calcium orthophosphate hydroxide, with chemical formula Ca₁₀(PO₄)₆(OH)₂, virtually insoluble in water and in many aqueous solvents. It is found as a mineral in phosphate rock. It is the principal inorganic constituent of bone matrix and teeth, which provides rigidity to these structures, and consists of hydrated calcium phosphate. Chemically prepared hydroxyapatite is useful in the separation of proteins or nucleic acids by adsorption chromatography. It is utilized in orthopedic and dental prostheses and in the prevention of osteoporosis (a disease of bones that leads to an increased risk of fracture). Unlike the other calcium phosphates, hydroxyapatite does not collapse under physiological conditions. In fact, it is thermodynamically stable at physiological pH and actively takes part in bone bonding, forming strong chemical bonds with surrounding bone. This characteristic has been exploited for rapid bone repair after major trauma or surgery. Hydroxyapatite (HA) is a biologically active calcium phosphate ceramic that is used in surgery to replace and mimic bone. While HA's bioactivity means it has a significant ability to promote bone growth alongside its surface, its mechanical

<http://www.ijesrt.com>

properties are inadequate for major load bearing devices [1]. The mineral component in the living bone is also a hydroxyapatite, the so-called biological apatite. The amount of the biological apatite in bone is approximately 70% by weight.

Properties of hydroxyapatite

1. Mechanical Properties: From the mechanical point of view, calcium orthophosphate bio-ceramics appear to be brittle polycrystalline materials for which the mechanical properties are governed by crystallinity, grain size, grain boundaries, porosity and composition. It appears to be very sensitive to slow crack growth. For dense bio-ceramics, the strength is a function of the grain size. Finer grain size means materials have smaller flaws at the grain boundaries and thus are stronger than bio-ceramics with larger grain sizes. The mechanical properties decrease significantly with increasing content of an amorphous phase, micro-porosity and grain size, while a high crystallinity, low porosity and small grain size tend to give a higher stiffness, higher compressive and tensile strength and a greater fracture toughness. For example,

(C)International Journal of Engineering Sciences & Research Technology

fracture toughness of HA bio-ceramics does not exceed $\sim 1.2 \text{ MPa}\cdot\text{m}^{1/2}$ (human bone: $2\text{--}12 \text{ MPa}\cdot\text{m}^{1/2}$). It decreases almost linearly with increasing porosity. Generally, fracture toughness increases with decreasing grain size. Though, in some materials, especially non-cubic ceramics, fracture toughness reaches the maximum and rapidly drops with decreasing grain size. For example, when the fracture toughness of pure hot pressed HA was investigated with grain sizes of $0.2\text{--}1.2 \mu\text{m}$, There appeared to be two distinct trends, where fracture toughness decreased with increasing grain size above $\sim 0.4 \mu\text{m}$ and subsequently decreased with decreasing grain size. The maximum fracture toughness measured was $1.20 \pm 0.05 \text{ MPa}\cdot\text{m}^{1/2}$ at $\sim 0.4 \mu\text{m}$. Fracture energy of HA bio-ceramics is in the range of $2.3\text{--}20 \text{ J/m}^2$, while the Weibull modulus is low ($\sim 5\text{--}12$) in wet environments, which means that HA behave as a typical brittle ceramics and indicates low reliability of HA implants [2]. Bending, compressive and tensile strengths of dense HA bioceramics are in the range of $38\text{--}250 \text{ MPa}$, $120\text{--}900 \text{ MPa}$ and $38\text{--}300 \text{ MPa}$, respectively. Similar values for porous HA bio-ceramics are in the range of $2\text{--}11 \text{ MPa}$, $2\text{--}100 \text{ MPa}$ and $\sim 3 \text{ MPa}$, respectively [2]. These wide variations in the properties are due to both structural variations (e.g., an influence of remaining microporosity, grain sizes, presence of impurities, etc.) and manufacturing processes, as well as caused by a statistical nature of the strength distribution.

2. **Electrical Properties:** Sometimes, electrical properties of calcium orthophosphate bioceramics are also studied. For example, a surface ionic conductivity of both porous and dense HA bioceramics has been examined for humidity sensor applications, since the room temperature conductivity is influenced by relative humidity. The ionic conductivity of HA has been a subject of research for its possible use as a sensor to alcohol, carbon dioxide or carbon monoxide gas. Electrical measurements have also been used as a characterization tool to study the evolution of microstructure in HA [2]. Interestingly, the electrical properties of calcium orthophosphate appear to influence their biomedical applications. For example, there is an interest in polarization of HA to

generate a surface charge by the application of electric fields at elevated temperatures [2]. The presence of surface charges on HA has shown to have a significant effect on both in vitro and in vivo crystallization of biological apatite. Moreover, growth of both biomimetic calcium orthophosphates and bones was found to be accelerated on negatively charged surfaces and decelerated on positively charged surfaces. The dielectric properties of hydroxyapatite has been examined to understand the decomposition of HA to tri-calcium phosphate (TCP) ($\text{Ca}_3(\text{PO}_4)_2$) as a result of the dehydration of hydroxyl ions at elevated temperatures since TCP is thought to have higher bioactivity than HA, but is also more biodegradable [2].

3. **Possible Transparency:** Single crystals of all calcium orthophosphates are optically transparent for visible light [2]. As bioceramics of calcium orthophosphates have a polycrystalline nature with a random orientation of big amounts of small crystals they are opaque and of white colour, unless coloured dopants have been added. But, in some cases, transparency is convenient to provide some essential advantages (e.g., to enable direct viewing of living cells in a transmitted light). Thus, sometimes transparent calcium orthophosphate bioceramics are prepared.
4. **Bioactivity:** Bioactivity is the ability of the material to directly bond to bone through chemical interaction and not physical or mechanical attachment. Bioactivity has been characterized in vitro and in vivo as the ability of the material to form carbonate apatite (similar to bone apatite) on its surface [3].
5. **Osteoconductive property:** Bioactive materials (calcium phosphates and bioactive glasses) also have osteoconductive properties – an ability to serve as a scaffold or template to guide the newly forming bone along its surfaces. Osteoconductive materials allow bone cell attachment, proliferation, migration and phenotypic expression, leading to formation of new bone in direct apposition to the biomaterial, thus creating a uniquely strong interface [3].
6. **Porosity:** Porosity is defined as the percentage of void spaces in solids and it is a morphological property independent of the material. The surface area of porous body is

much higher, which guarantees a efficient mechanical fixation in addition to providing sites on the surface that allow chemical bonding between the bioceramics and bones [2]. Furthermore, a porous material may have both closed (isolated) pores and open (connected) pores. Connected pores appear as tunnels and are accessible by gases, liquids and particulate suspensions. Moreover, dimensions of open pores are directly related to bone formation, since such pores grants both the surface and space for cell adhesion along with bone growth. On the other hand, pore interconnection provides the way for cell distribution and migration. Namely, porous HA bio-ceramics can be colonized by

bone tissues. Therefore, interconnecting macro porosity (pore size $>100 \mu\text{m}$), which is defined by its capacity to be colonized by cells, is intentionally introduced in solid bioceramics (Figure 1). Macro porosity is usually formed due to a release of various volatile materials and, for that reason, integration of pore-creating additives (porogens) is the most popular technique to create macro-porosity. The porogens are crystals or particles of either volatile (they evolve gases at elevated temperatures) or soluble substances, such as paraffin, naphthalene, sucrose, NaHCO_3 , gelatine, polymethylmethacrylate or even hydrogen peroxide[2].

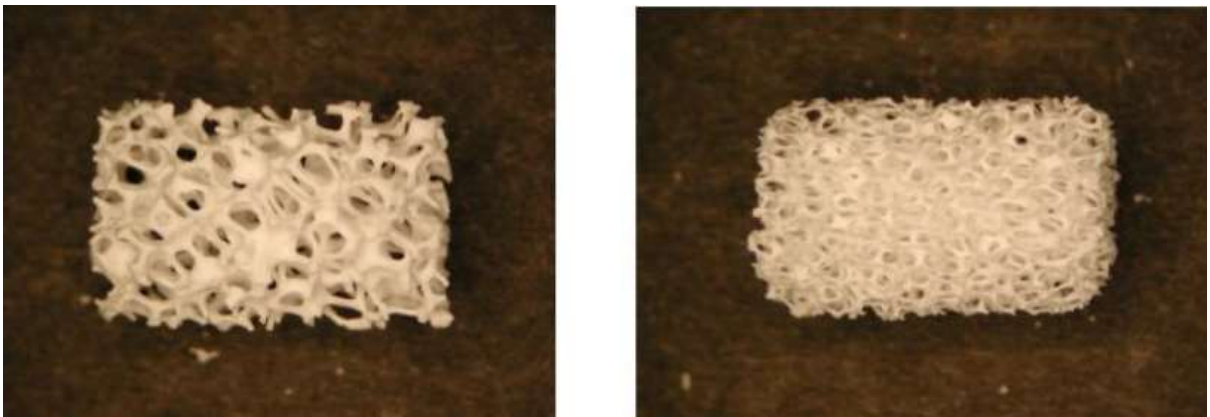


Figure 1. Photographs of a commercially available porous calcium orthophosphate Bio-ceramic with different porosity.

Applications of Hydroxyapatite: Due to high brittleness (associated to a low crack resistance), biomedical applications of calcium orthophosphate bio-ceramics are focused on production of non-load bearing implants, such as pieces for middle ear surgery, filling of bone defects in oral or orthopaedic surgery, as well as coating of dental implants and metallic prosthesis.

Applications include dental implants, percutaneous devices and use in periodontal treatment, healing of bone defects, fracture treatment, total joint replacement (bone augmentation), orthopaedics, cranio-maxillofacial reconstruction, otolaryngology and spinal surgery. Depending upon the required properties, different calcium orthophosphates might be used.

Generally HA can be used in the following forms:

- 1. Implant Coatings:** Coatings of hydroxyapatite are often applied to metallic implants (most commonly titanium/titanium alloys and stainless steels) to alter the surface properties of the materials. In this manner the body sees hydroxyapatite-type material to which it accepts without any problem. Without the coating the body would see a foreign body and work in such a way as to isolate it from surrounding tissues. At present, the only commercially accepted method of applying hydroxyapatite coatings to metallic implants is plasma spraying [4].
- 2. Bone Fillers:** Hydroxyapatite may be employed in forms such as powders, porous blocks or beads to fill bone defects or voids. These may arise when large sections of bone have had to be removed (e.g. bone cancers) or when bone augmentations are required

(e.g. maxillofacial reconstructions or dental applications). The bone filler will provide a scaffold and encourage the rapid filling of the void by naturally forming bone and provides an alternative to bone grafts. It will also become part of the bone structure and will reduce healing times compared to the situation, if no bone filler was used [4].

3. **HA as Abrasive:** A rough surface of Ti or Ti alloy implant was reported to promote greater osteointegration reflected by stronger bone-implant interface. Implant surface roughening accomplished by grit-blasting with abrasives, usually silica or alumina. More recently HA or apatite abrasive (biphasic calcium phosphate) has gained popularity as the abrasive of choice for orthopedic and dental. Implant surface grit-blasted with HA or apatite abrasive appears to be cleaner (free of inclusions) compared with alumina and appear to promote higher bone contact [3].

Experimental Procedure: In this section, the design and working of experimental setup used for preparation and characterization of hydroxyapatite have been described. In addition, the detailed sample preparation procedure and procedure employed for X-ray diffraction (XRD), Scanning Electron Microscopy (SEM) and weight loss measurements by Thermogravimetric Analysis (TGA) are given in details.

Sample Preparation: Several methods have been utilized for the synthesis of HAP, which includes

precipitation technique, sol-gel method, hydrothermal technique, multiple emulsion technique, biomimetic deposition technique, electro-deposition technique etc. In present study the sol-gel method as suggested by Agrawal *et al.* [5] has been used to prepare hydroxyapatite powder (HA) and HA-CNT composite. The following materials were used as raw materials or starting materials.

(a) Phosphoric Pent-oxide P_2O_5 ;
molecular weight \rightarrow 141.94 g/mol

(b) Calcium nitrate tetra-
hydrate $Ca(NO_3)_2 \cdot 4H_2O$; molecular
weight \rightarrow 236.15 g/mol

At first phosphoric pentoxide (P_2O_5) is dissolved in absolute ethanol to form a 0.5 mol/litre solution and secondly calcium nitrate tetrahydrate ($Ca(NO_3)_2 \cdot 4H_2O$) is also dissolved in ethanol to form 1.67 mol/litre solution. After this, both the solutions are mixed to obtain the desired Ca/P molar ratio of 1.67.

The whole procedure of preparing the HA powder is as shown in the following flow diagram (Figure 2).

For making the solution of 1 mol/litre concentration of $Ca(NO_3)_2 \cdot 4H_2O$ we need 236.15 g of calcium nitrate tetrahydrate in 1 litre ethanol as according to the molecular weight of $Ca(NO_3)_2 \cdot 4H_2O$, one mol is equivalent to 236.15 g. Correspondingly for making 1.67 mol/litre solution we need 394.37 g of calcium nitrate tetrahydrate in one litre of ethanol. In the same way we need 70.97 g of phosphoric pentoxide in one litre of ethanol to form 0.5 mol/litre solution.

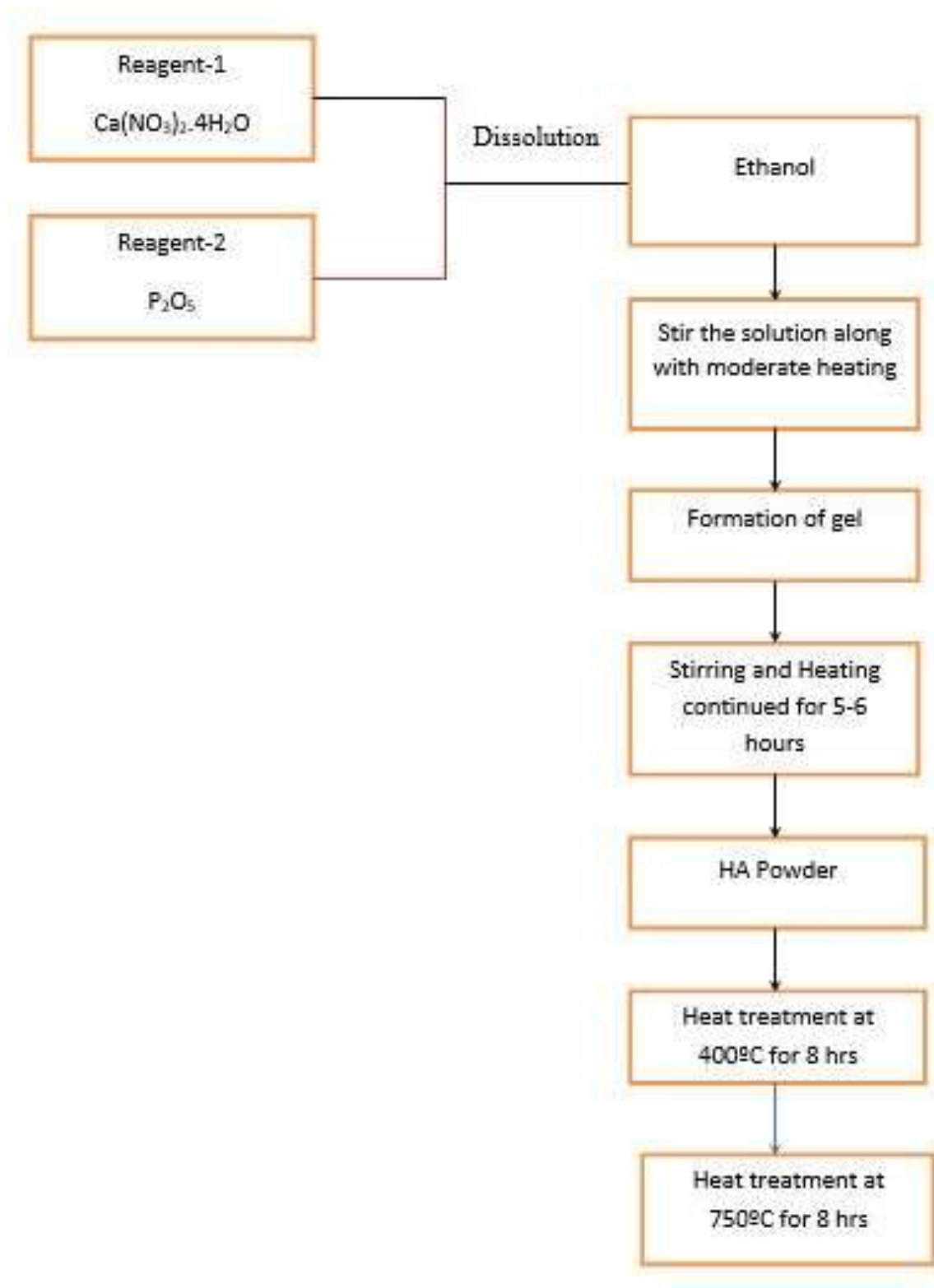
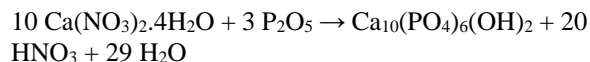


Figure 2 Schematic flow process chart for the synthesis of HA powder by the use of $\text{Ca}(\text{NO}_3)_2 \cdot 4\text{H}_2\text{O}$ and P_2O_5

The sample was prepared by dissolving both the chemicals into 50 ml ethanol. So accordingly the required amount of the chemicals were calculated which appeared to be as follows:

- Calcium nitrate tetrahydrate ($\text{Ca}(\text{NO}_3)_2 \cdot 4\text{H}_2\text{O}$) \rightarrow 19.72 g in 50 ml ethanol.
 - Phosphoric pentoxide (P_2O_5) \rightarrow 3.54 g in 50 ml ethanol.
1. First of all the calculated amount of calcium nitrate tetrahydrate and phosphoric pentoxide were dissolved in 50 ml ethanol each in two separate 100 ml beakers. Then both the solutions were mixed together gradually into a 250 ml beaker.
 2. After that the solution was stirred by using magnetic stirring needle for 15-20 minutes.
 3. Then heating was also started along with stirring and the temperature was kept around 70°C.
 4. So during stirring and heating the gel was formed after near about 2 hours and after 6-7 hours the powder was formed in a dry condition.
 5. This powder was taken out of the beaker and grinded for homogeneous distribution of particles throughout the powder.
 6. Further this powder was sintered at 400°C and 750°C for 8 hours separately.

The chemical reaction occurred during the above process is as given below:



The nitric acid and water are the by-products of the reaction.

Some samples of HA powder obtained in first step i.e. without any sintering were also washed with distilled water by using laboratory bench-top centrifuge. The sample was washed three times and time for each washing given in the centrifuge was 10 minutes at 3400 rpm. A significant part of the powder used for washing was lost during the washing process. For illustration, 8.51 g powder was used for washing and 6.96 g powder was lost during the washing and only 1.55 g powder was obtained after washing and drying it. So it was observed that almost 82% powder has been lost in the washing process.

Another sample was prepared by embedding the CNTs into the powder i.e. HA-CNT composite. CNTs were embedded just 15-20 after the stirring was started and rest of the procedure was same as mentioned above. CNTs were in powder form and 20 mg CNTs were mixed into the solution of the earlier mentioned calculations. Figure 3 shows the schematic flow process chart for the synthesis of HA-CNT composite by the use of $\text{Ca}(\text{NO}_3)_2 \cdot 4\text{H}_2\text{O}$ and P_2O_5 .

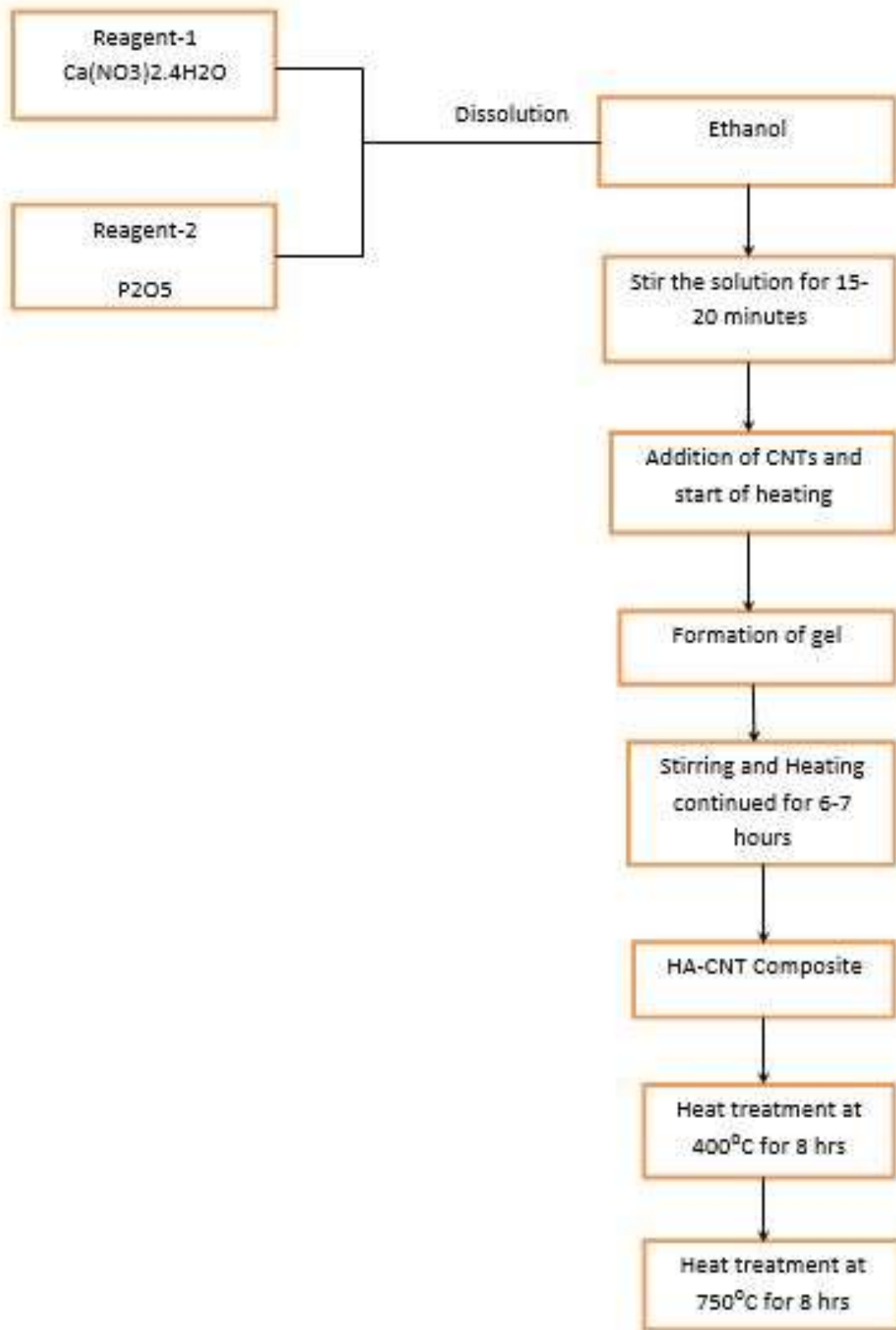


Figure 3 Schematic flow process chart for the synthesis of HA powder by embedding CNT's

Details and Labels of Various Samples:

Sample 1 HA powder sample without any heat treatment and washing.

Sample 2 HA powder sample washed and sintered at 400°C for 8 hours.

Sample 3 HA powder sample washed and sintered at 750°C for 8 hours.

Sample 4 HA-CNT composite powder sample washed and sintered at 750°C for 8 hours.

Results and discussion

X-ray diffraction (XRD) Analysis of Sample: In order to confirm the crystalline nature of the HA sample & to find the change in its crystallinity after sintering, X-ray diffraction study had been made on HA samples using Cu K α radiation ($\lambda = 1.5418 \text{ \AA}$). X-ray Diffraction (XRD) is a powerful non-destructive

technique for characterizing crystalline materials. It provides information related to structures, phases, preferred crystal orientations, and other structural parameters, such as crystallinity, strain. X-ray diffraction peaks are produced by constructive interference of monochromatic beam of x-rays scattered at specific angles from each set of lattice planes in a sample. The phenomenon is called X-ray diffraction.

Figure 4 shows the typical X-ray diffraction pattern of the HA powder washed and sintered at 400°C for 8 hours. The X-ray pattern of this sample possessed the characteristic hump. This hump in the XRD pattern reveals the “amorphous” nature of the sample. Ungureanu et al. [6] have reported that the nano powder of hydroxyapatite converted into crystalline phase above 200°C. The crystallinity increases with increasing heating temperature.

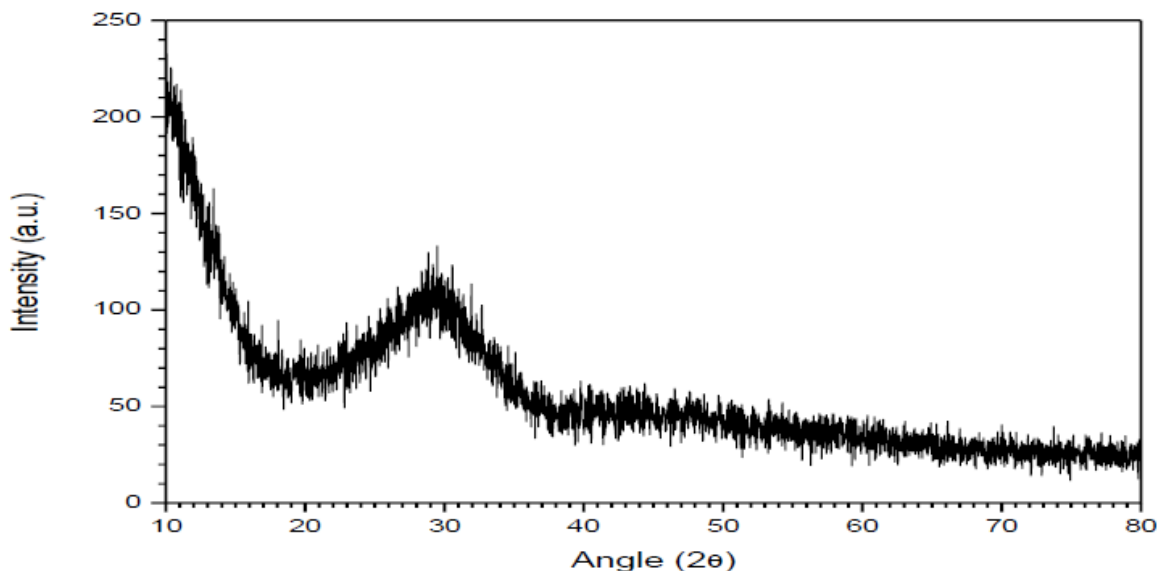


Figure 4 XRD Pattern for Sample 2

Figure 5 shows the XRD pattern of sample 3, washed and sintered at 750°C for 8 hours. Similarly, the XRD pattern of sample 4 i.e. the HA-CNT composite powder washed and sintered at 750°C for 8 hours is also shown in figure 4.2. For sample 3 the peaks positioned at 31.63°, 29.72° and 27.80° were indexed to (221), (-132) and (-112) crystal planes, respectively. These three peaks and the other peaks marked as “+” are indexed to the hydroxyapatite, (ICDD card No. 01-

089-4405). It is the main phase formed with the monoclinic crystal lattice. The volume fraction of hydroxyapatite was observed to be 68% in sample 3 as marked as phase A.

Except the HA powder, calcium phosphate hydrate was also present in the powder as shown in figure 5. The secondary phase has been indexed to calcium phosphate hydrate (ICDD card No. 01-070-4788). This phase has been represented as phase B and the volume fraction of this phase is found 32%.

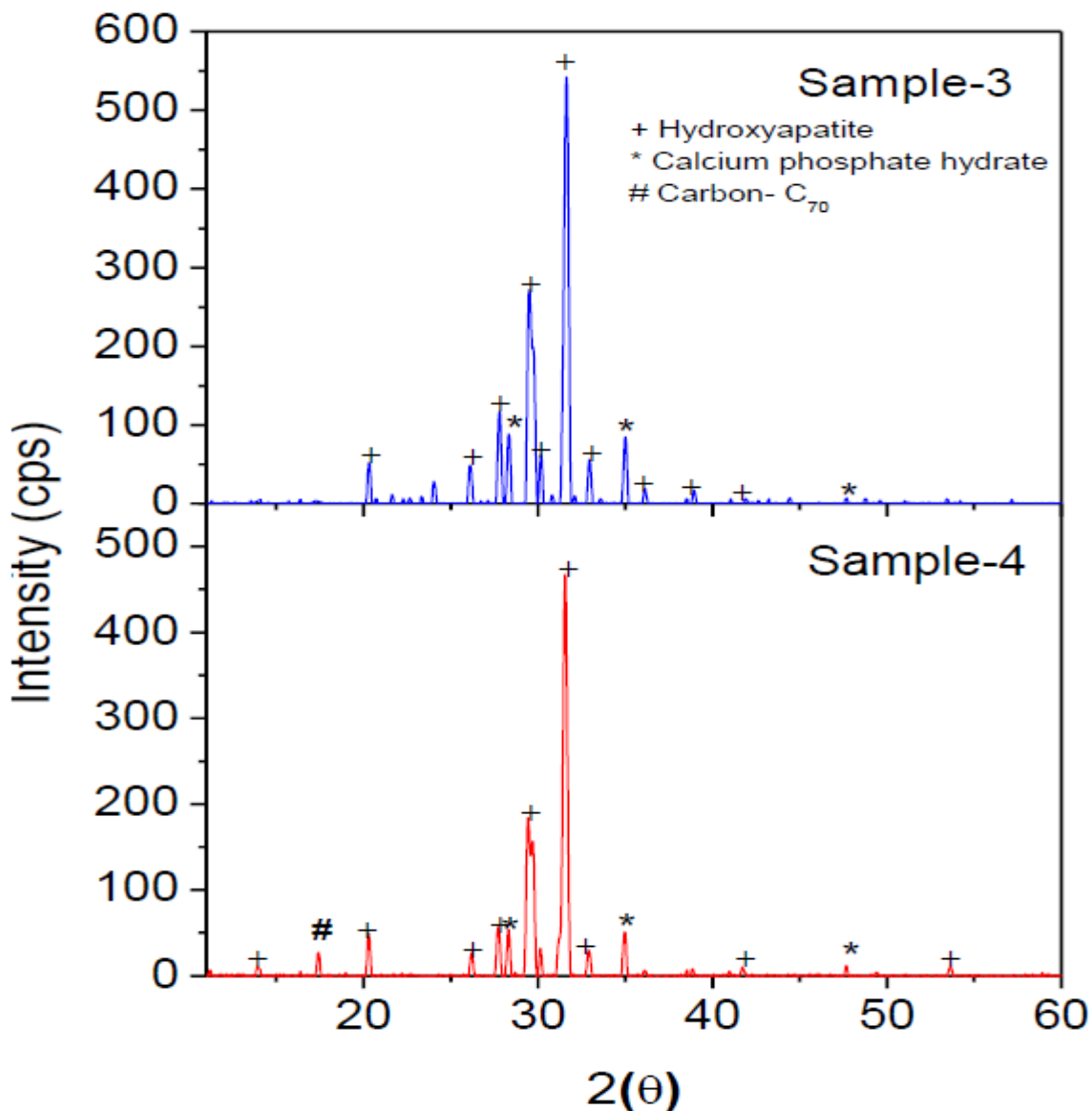


Figure 5 XRD pattern of the sample 3 and 4.

As compared to Sample 3, the addition of CNTs in sample 4 leads to the shifting of XRD peaks towards lower diffraction angle which indicates the presence of some tensile stress in the sample. It may be attributed due to occupation of interstitial sites in the lattice of HA phase by carbon. The following table 1 describes the diffraction angle according to peaks observed, phase present and crystal plane for each peak for sample 3.

Table 1 Diffraction data for sample 3.

2θ (degrees)	Phase	(hkl)
13.93	A	(011)
20.31	A	(031)
26.10	A	(012)
27.80	A	(-112)
28.31	B	(220)
29.72	A	(-132)
30.17	A	(051)
31.63	A	(221)
32.94	A	(060)
34.99	B	(-223)
41.91	A	(161)
47.69	A	(133)
53.42	A	(-114)

For sample 4 the peaks positioned at 31.54°, 29.71° and 27.72° were indexed to (221), (-132) and (-112) crystal planes, respectively. These peaks and the other peaks marked as “+” in the pattern are indexed to the hydroxyapatite powder as per ICDD card No. 01-089-4405. Like in sample 3, in this sample also, it is main phase with 67% volume fraction of this phase and denoted as phase A. The other phase present, as secondary phase, was calcium phosphate hydrate. The

secondary phase has been indexed to calcium phosphate hydrate (ICDD card No. 01-070-4788). The volume fraction of this phase is 31% in the concerned sample. Furthermore, due to addition of CNTs, some traces of carbon were also seen in the XRD pattern as shown by the marked peak positioned at 17.42° in the XRD pattern of sample 4. Carbon has been designated as phase C and its volume fraction is about 2%.

Table 2 Diffraction data for sample 4.

2θ (degrees)	Phase	(hkl)
13.93	A	(011)
17.42	C	(130)
20.29	A	(031)
26.20	A	(012)
27.72	A	(-112)
28.31	B	(220)
29.71	A	(-132)
30.15	A	(051)
31.54	A	(221)
32.90	A	(060)
34.96	B	(-223)
41.71	A	(161)
47.68	B	(133)
53.61	A	(-114)

The XRD patterns were also used to calculate the crystallite size of both the samples using classical Scherer equation.

$$D = \frac{0.9\lambda}{\beta \cos\theta} \dots\dots\dots(2)$$

Where D is crystallite size, λ is wave length of incident x-ray, β is Full Width at Half Maximum (FWHM) and θ is the half of the diffraction angle of the corresponding peak. The comparison between crystallite size of sample 3 and 4 has been shown in table 3. The crystallite size is around 31 nm for sample 3. On the other hand, sample 4 exhibits larger crystallite size i.e. around 36 nm. It is also evident from XRD pattern as peaks are sharper in sample 4 than sample 3. The addition of CNTs enhance the crystallinity as crystallite size changes from 31 nm to 36 nm. The crystallite size of HA phase is more or less similar order as reported by Ungureanu et.al. [6] for HA phase which was synthesized by chemical precipitation method.

Table 3 Crystallite size of sample 3 and 4.

	Sample 3	Sample 4
λ(Å)	1.54	1.54
FWHM (radians)	4.595×10-3	4.054×10-3
θ (radians)	0.2764	0.2754
Cosθ	0.9620	0.0.962
Average Crystallite size (nm)	31	36

Thermal Analysis (TGA-DTA) of Sample: The TGA curve of as prepared sample i.e. sample 1 is shown in figure 6. The sample has not been given any heat treatment before the TGA analysis. The TG curve could not show sharp defined steps as reported by Hui et.al. [7]. The pattern shows that there is weight loss of about 20% up to 70°C which may be mainly due to loss of absorbed water content and approximately 30% weight loss has been observed in the temperature range of 70°C to 350°C. Further, about 6% weight loss was observed in the range of 350°C to 500°C. Beyond 500°C to 1000°C no significant weight loss was observed. Almost stable curve was observed in this temperature range.

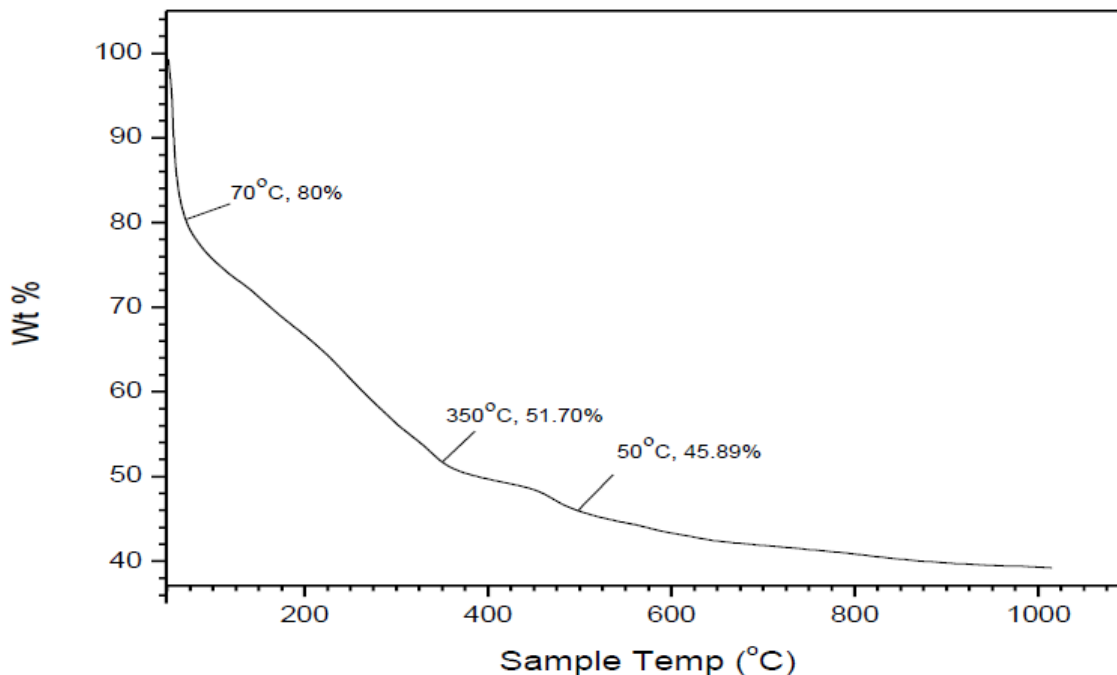


Figure 6 TGA pattern of the sample 1.

The heat treated and CNT added sample shows better thermal stability as compared to as prepared sample as shown in figure 6. TGA analysis shows that there is weight loss of about 0.5% up to temperature 200°C. This loss is mainly due to loss of the absorbed water content. Further another weight loss of about 1.54% has been observed in the temperature range of 240°C to 600°C. This weight loss may be due to evaporation of some volatile substances present in the powder. This weight loss can be seen as the result of increased crystallinity of the powder. Further, beyond 600°C, the powder showed a continuous weight loss with respect

to temperature which is mainly due to the carbon loss from the powder which was present because of embedding of CNTs in to the sample. This continuous decrease in the weight indicates that the prepared powder does not possess thermal stability.

In comparison to as prepared sample TGA, the sample 4 curve shows better stability. The less slope becomes more clear. The heat treated sample is melted at 1150°C as observed in figure 7.

The melting point of HA is 1100°C. It is reported in the same range as observed in the present sample.

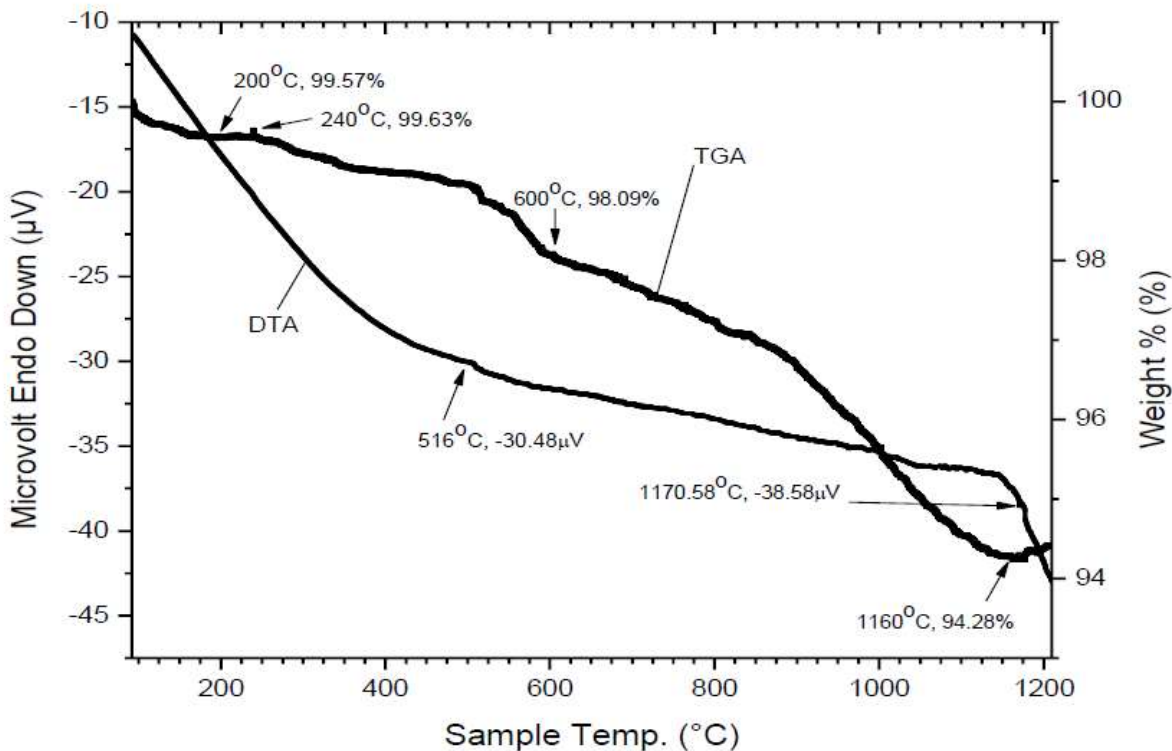


Figure 7 TGA-DTA pattern of the sample 4.

The DTA curve of this sample shows a broad exothermic peak started at ~1150°C. It might belong to the melting of HA layer.

SEM and EDS Analysis of Sample: Figure 8 shows the SEM image of sample 3 which was sintered at 750°C for 8 hours. These images were taken in

secondary emission mode. The image reveals the formation of HA powder made up of agglomeration of nano sized grains. The grains may be agglomerated due to the formation of gel during the synthesis process.

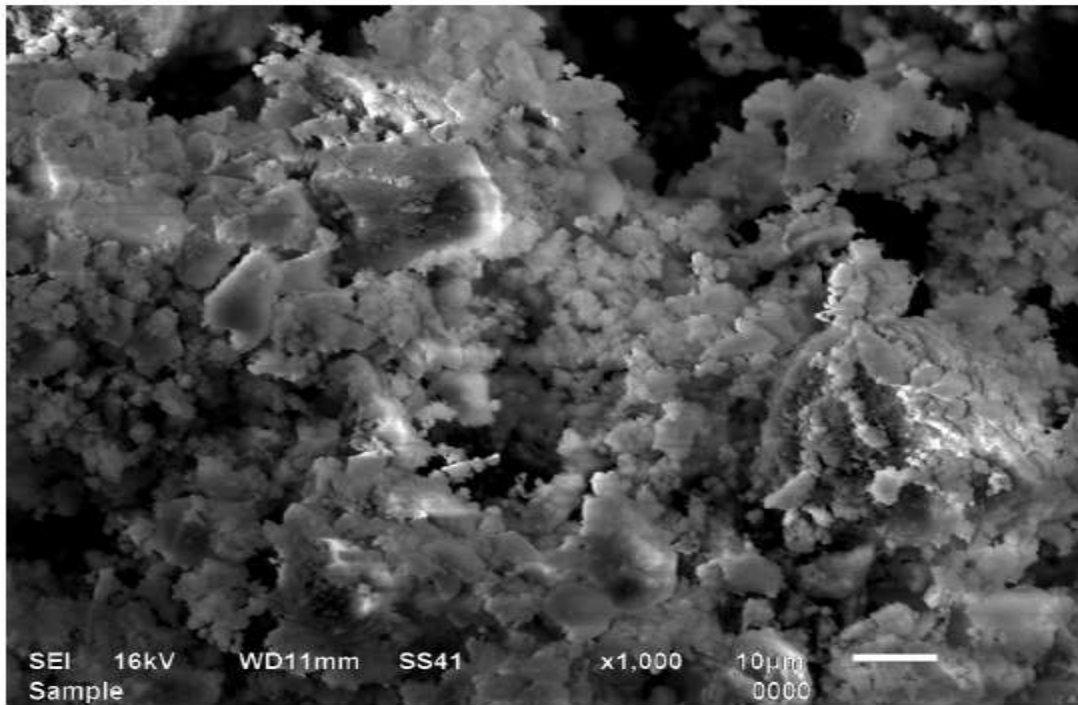


Figure 8 SEM micrograph of sample 3.

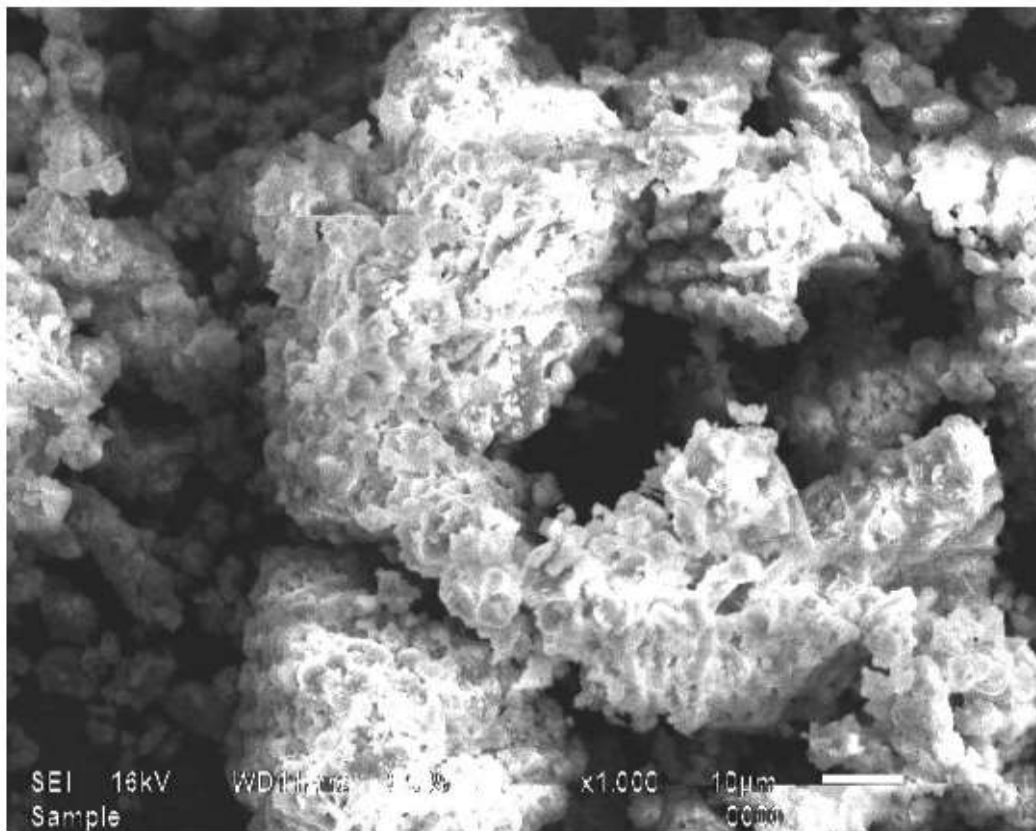


Figure 9 SEM micrograph of sample 4.

Figure 9 shows the SEM image of sample 4 i.e. HA-CNT composite which was sintered at 750°C for 8 hours. Due to agglomeration, it is very difficult to estimate the particle size. The shapes of the particles are either spherical or semi-spherical. The agglomeration tendency is more pronounced in sample 4 as compared to sample 3 as shown in figure 4.5 and 4.6. Moreover, the agglomeration of the crystallites leaves bigger pores as observed in these figures. Sometimes, the porosity in biomaterials is beneficial

to permit the circulation of body fluid when it is used as implants [2].

The EDS was also performed on the sample 3 and sample 4 to check the weight percentage of different elements present in these samples. The theoretical weight percentage of various elements present in the powder was calculated with the help of XRD pattern of the samples and the practical weight percentage was observed from EDS spectrum of the samples. These two values were compared with each other.

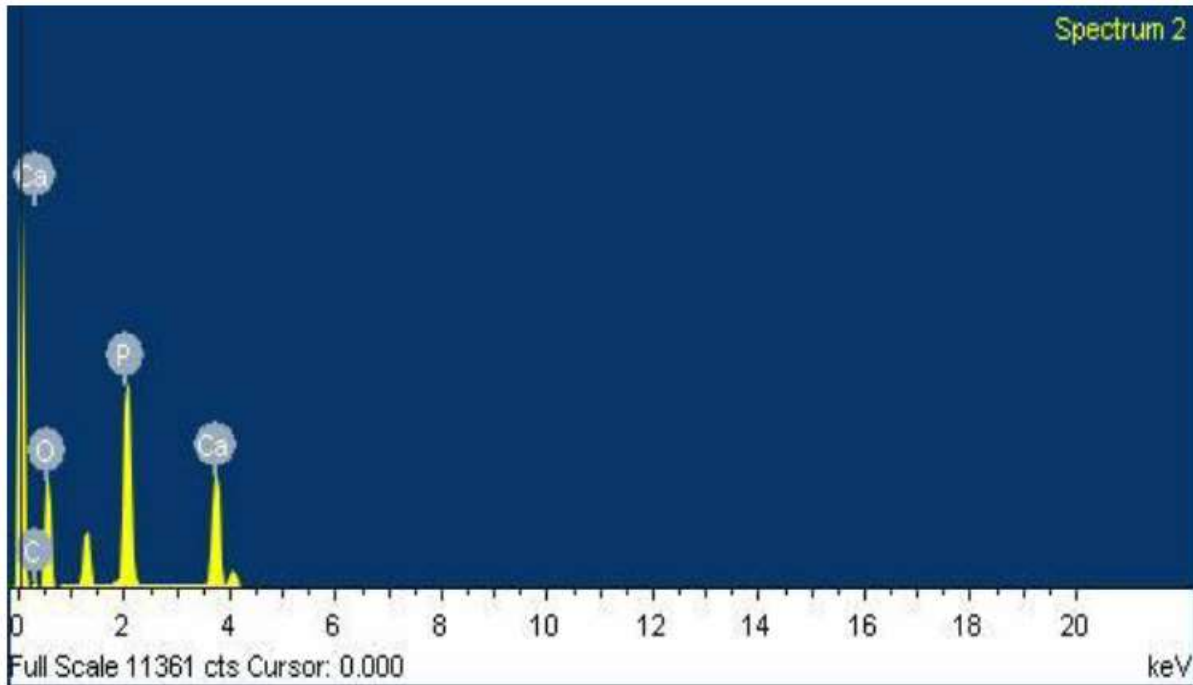


Figure 10 EDS spectrum of sample 3.

Figure 10 shows the EDS spectrum of sample 3 which was sintered at 750°C for 8 hours. Some carbon content had been observed which may be present due to grid beneath the sample.

Table 4 shows the comparison between theoretical and practical weight percentage of elements in sample 3.

Element	Element Theoretical Weight %age	Experimental Weight %age
Ca	36.31	19.01
P	19.34	21.51
O	44.35	59.48

Table 4 Elemental weight percentage comparison for sample 3.

Figure 11 shows the EDS spectrum of sample 4 i.e. HA-CNT composite which was sintered at 750°C for 8 hours. Table 5 shows the comparison between theoretical and experimental weight percentage of elements in sample 4. The EDS analysis clearly indicates the presence of Ca, P, O and C, which are present in hydroxyapatite phase.

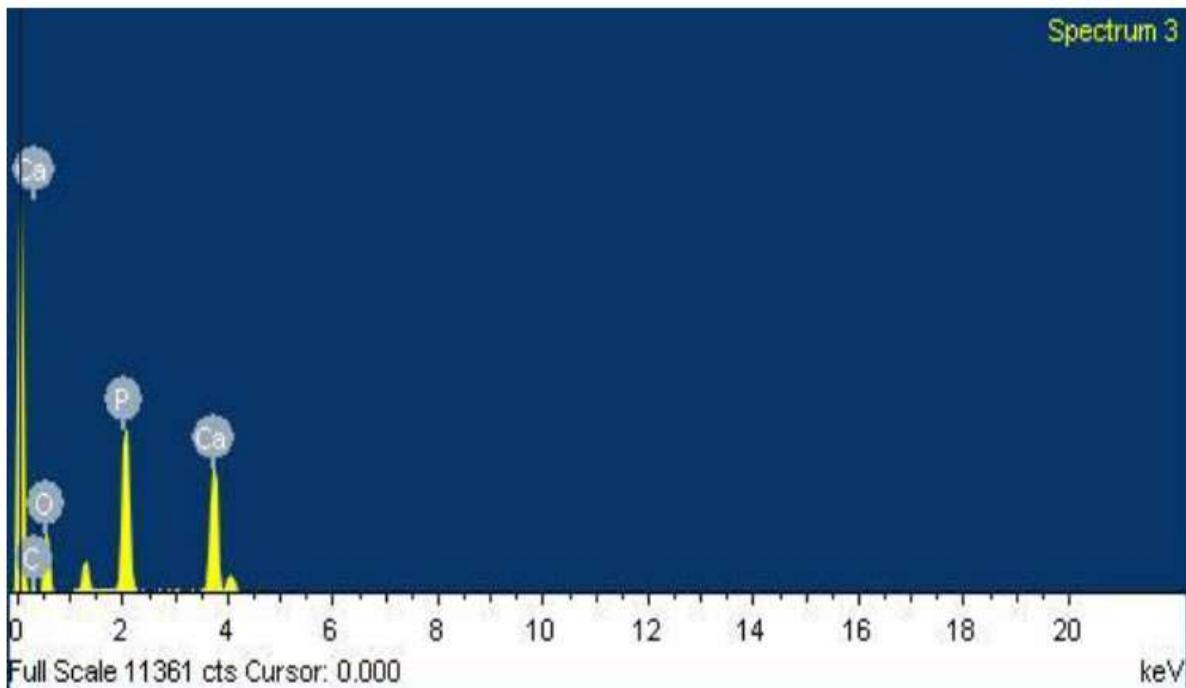


Figure 11 EDS spectrum of sample 4.

Table 5

Element	Theoretical Weight %age	Experimental Weight %age
Ca	35	23.10
P	17.92	19.79
O	42.66	50.72
C	4.42	6.39

Conclusion

In the present study, the samples are prepared by sol-gel technique. The as prepared samples show the amorphous nature. The higher temperature heat treatment (750°C/8 hours) leads to the formation of HA and hydrate phase. The volume fraction of these phases is 67% and 31% respectively. The addition of CNTs, in as prepared and heat treated samples, increased the crystallinity and thermal stability along with crystallite size. The SEM study clearly shows the agglomeration with higher porosity. The melting point is observed ~1150°C. EDS analysis clearly shows the presence of hydroxyapatite and related phase. However, these phases are chemically non-stoichiometric as calculated from the weight percentage of different elements.

References

1. A. A. White and S. M. Best, International Journal of Applied Ceramic Technology 4(1) (2007), 1-13.
2. S. V. Dorozhkin, Calcium orthophosphates as bioceramics: state of the art, Journal of Functional Biomaterials. 1 (2010), 22-107.
3. T. Kokubo, Bioceramics and their clinical applications, JMM, Woodhead Publishing Limited (2008).
4. <http://www.azom.com>
5. K. Agrawal, G. Singh, D. Puri, S. Prakash, Journal of Minerals & Materials Characterization & Engineering, 10(8) (2011), 727-734.
6. D. N. Ungureanu, N. Angelescu, R. M. Ion, E. V. Stoian, C. Z. Rizescu, Recent Researches in Communications, Automation, Signal Processing, Nanotechnology, Astronomy and Nuclear Physics (Published in proceeding) (2011), 296-391.
7. P. Hui, S.L. Meena, G. Singh, R.D. Agarawal, S. Prakash, Journal of Minerals & Materials Characterization & Engineering, 9 (8) (2010), 683-692.